24 August 1973, Volume 181, Number 4101 **SCIENCE**

Tubular Packing of Spheres in Biological Fine Structure

Protein monomers of viruses, flagella, and microtubules form patterns like those of leaves of plants.

Ralph O. Erickson

High resolution electron microscopy, x-ray diffraction, and some other techniques are providing detailed information on the ultrastructure of a number of biological structures that are assembled from protein monomers. One class of such structures is cylindrical tubules, such as the protein coats of some viruses, flagella of bacteria such as *Salmonella*, and a variety of microtubules. Microtubules are found in the mitotic spindle of higher organisms, as supporting elements in many nonspherical cells, such as the heliozoan protozoa, and are also thought to play a part in the synthesis or assembly of other structural components of cells.

There is little consistency in the geometric conventions which various authors have used in describing these structures, perhaps because the underlying geometry has not been thoroughly understood. In most cases, the symmetry of arrangement of the monomers into the larger structure is obviously helical. Therefore, some authors have given the pitch and diameter of certain evident helices, as is done in specifying a screw in practical mechanics. Others have centered their attention on the number of monomers which appear in a cross section, and spoken of 11-, 12- or 13-stranded filaments. It is understandable that the conventions of crystallography are used in describing the results of x-ray and optical diffraction studies of these structures. The descriptive considerations may be related to theories of the mechanism of assembly and disassembly of the structures. For instance, it has been proposed that a microtubule may be assembled by the coiling up of one or more previously assembled protofilaments, and there are references to four-start and five-start helices.

To my naive eye, the salient property of these structures is the hexagonal packing pattern of the monomers; this has also been the view of several other authors. The symmetry of hexagonal packing in an extended plane is elementary, and is described by Coxeter (*1*), for instance, as corresponding to one of the possible tessellations in the plane. While the cylinder is a developable surface, in that it can be unrolled into a plane, still a new element enters into symmetrical patterns on a cylindrical surface, since the symmetry must be unbroken about the circumference. The geometry of these patterns has been worked out exhaustively by Iterson (*2*) as a part of his mathematical study of phyllotaxis. I propose that Iterson's models, specifically of the packing of spheres on the surface of a cylinder, be used as the basis for descriptions of these aspects of ultrastructural symmetry. The classical terminology of phyllotaxis, in particular the terms parastichy for any rank of subunits, and angular divergence from one subunit to the next, are as completely appropriate to ultrastrucural patterns as they are to the arrangement of leaves on the stem of a higher plant, or scales on a pine cone.

In this article I review and extend Iterson's (*2*) geometry in the restricted case of the arrangement of spheres, whose centers lie on the surface of a circular cylinder, such that each sphere is in contact with six others. Probably because of the difficulty of calculating by successive approximation, Iterson tabulated only a few patterns. He chose examples corresponding to existing patterns of leaf arrangement in higher plants, and it appears that other patterns occur at the ultrastructural level. Computer solutions of Iterson's equations are given here, together with drawings of some patterns. Several patterns displayed by submicroscopic biological structures are analyzed in these terms.

Derivation of Equations

It will be useful first to consider symmetrical patterns of points on a cylindrical surface. In Fig. 1, a point set which is characterized by screw symmetry is illustrated. The basic symmetry operation, congruence (*3*), or isometry (*1*) is the screw displacement or twist, which is the product of a rotation and a translation parallel to the axis. One such isometry would transform point 0 into point 1. Other screw displacements can also be considered, such as 0 to 5, 0 to 13, and an unlimited number of others. Alternatively, one can visualize ranks of points as arranged along helices, and these will be referred to as parastichies. Just as in an orchard where trees are arranged in rows in many directions, many parastichies can be traced through the points. In general, the parastichies are helices, although in the limiting cases they are circles (whorls), or vertical

---

The author is professor of botany at the University of Pennsylvania, Philadelphia 19174.

generators of the cylinder (orthostichies). Certain parastichies are subjectively more evident than others. It is convenient to specify a given pattern by citing the two or three sets of evident parastichies, which are of intermediate pitch, connect nearest points, intersect most nearly at right angles, or have some other stated property.

Cylindrical patterns of points may be constructed so that all points fall on a single generative helix, or 1-parastichy. In this case only one point occurs at a given distance along the length of the cylinder, or, if the circular circumference of the cylinder were drawn through a given point, it would pass through no other point. In

Table 1. Parameters of models of hexagonally packed spheres of unit radius, whose centers are on a circular cylinder, classified by number of strands or near-longitudinal parastichies.

Contacts $k(m, n, m + n)$	Divergence		Vertical displacement h	Radius of cylinder R	Inclination of parastichies		
	α (degrees)	δ_m (degrees)			μ (degrees)	ν (degrees)	ϕ (degrees)
			Three strands				
3(0, 1, 1)	60.0	120.0	1.6329931	1.1547005	0.000	−53.481	53.481
(1, 2, 3)	131.810320	131.810320	0.6324555	1.0392305	14.818	−35.889	71.289
			Four strands				
4(0, 1, 1)	45.0	90.0	1.6817928	1.4142136	0.0	−56.558	56.558
(1, 3, 4)	97.743120	97.743120	0.4693787	1.2905240	12.035	−43.116	69.617
2(1, 1, 2)	90.0	90.0	1.0	1.2247449	27.465	−27.465	90.0
			Five strands				
5(0, 1, 1)	36.0	72.0	1.7013016	1.7013016	0.0	−57.858	57.858
(1, 4, 5)	77.414817	77.414817	0.3719648	1.5712212	9.938	−47.144	68.238
(2, 3, 5)	−141.843980	76.312040	0.3960824	1.4862538	21.810	−34.954	81.963
			Six strands				
6(0, 1, 1)	30.0	60.0	1.7111994	2.0	0.0	−58.535	58.535
(1, 5, 6)	63.979611	63.979611	0.3075215	1.8651700	8.399	−49.688	67.156
2(1, 2, 3)	64.605543	64.605543	0.6513963	1.7692473	18.083	−39.716	77.684
3(1, 1, 2)	60.0	60.0	1.0	1.7320508	28.869	−28.869	90.0
			Seven strands				
7(0, 1, 1)	25.714286	51.428572	1.7169464	2.3047649	0.0	−58.933	58.933
(1, 6, 7)	54.468269	54.468269	0.2618672	2.1663703	7.246	−51.385	66.304
(2, 5, 7)	−152.220650	55.558700	0.2759292	2.0623138	15.427	−43.000	74.923
(3, 4, 7)	−102.114200	53.657400	0.2845311	2.0037630	24.460	−33.885	84.782
			Eight strands				
8(0, 1, 1)	22.50	45.0	1.7205911	2.6131259	0.0	−59.188	59.188
(1, 7, 8)	47.393551	47.393551	0.2278914	2.4719986	6.359	−52.623	65.622
2(1, 3, 4)	48.557790	48.557790	0.4781292	2.3615130	13.436	−45.394	72.950
(3, 5, 8)	135.960910	47.882730	0.2470401	2.2888251	21.179	−37.569	81.168
4(1, 1, 2)	45.0	45.0	1.0	2.2630334	29.363	−29.363	90.0
			Nine strands				
9(0, 1, 1)	20.0	40.0	1.7230522	2.9238044	0.0	−59.361	59.361
(1, 8, 9)	41.931568	41.931568	0.2016509	2.7805347	5.659	−53.556	65.069
(2, 7, 9)	−158.479760	43.040480	0.2107296	2.6648441	11.889	−47.210	71.452
3(1, 2, 3)	42.948100	42.948100	0.6533239	2.5817903	18.654	−40.374	78.506
(4, 5, 9)	−79.658580	41.365680	0.2217071	2.5377417	25.828	−33.168	86.098
			Ten strands				
10(0, 1, 1)	18.0	36.0	1.7247940	3.2360680	0.0	−59.484	59.484
(1, 9, 10)	37.590442	37.590442	0.1807896	3.0910831	5.094	−54.282	64.611
2(1, 4, 5)	38.604707	38.604707	0.3766097	2.9711125	10.654	−48.634	70.270
(3, 7, 10)	−107.068080	38.795760	0.1944493	2.8799837	16.654	−42.573	76.456
2(2, 3, 5)	−71.023387	37.953226	0.3970983	2.8223445	23.016	−36.178	83.092
5(1, 1, 2)	36.0	36.0	1.0	2.8025171	25.592	−25.592	90.0
			Eleven strands				
11(0, 1, 1)	16.363636	32.727273	1.7260729	3.5494655	0.0	−59.574	59.574
(1, 10, 11)	34.058980	34.058980	0.1638156	3.4030824	4.630	−54.864	64.227
(2, 9, 11)	−162.513870	34.972260	0.1701343	3.2795451	9.647	−49.772	69.311
(3, 8, 11)	131.766390	35.299170	0.1754887	3.1818903	15.033	−44.340	74.821
(4, 7, 11)	98.721924	34.887696	0.1794356	3.1136676	20.735	−38.606	80.710
(5, 6, 11)	−65.269777	33.651115	0.1815468	3.0783987	26.659	−32.668	86.870
			Twelve strands				
12(0, 1, 1)	15.0	30.0	1.7270401	3.8637033	0.0	−59.643	59.643
(1, 11, 12)	31.130975	31.130975	0.1497400	3.7161614	4.241	−55.339	63.901
2(1, 5, 6)	31.948959	31.948959	0.3102475	3.5896154	8.811	−50.715	68.517
3(1, 3, 4)	32.335872	32.335872	0.4794166	3.4865583	13.693	−45.790	73.485
4(1, 2, 3)	32.180692	32.180692	0.6539269	3.4098054	18.852	−40.602	78.775
(5, 7, 12)	150.281250	31.406250	0.1658479	3.3622191	24.225	−35.213	84.317
6(1, 1, 2)	30.0	30.0	1.0	3.3460652	29.717	−29.717	90.0
			Thirteen strands				
13(0, 1, 1)	13.846154	27.692306	1.7277895	4.1785815	0.0	−59.696	59.696
(1, 12, 13)	28.664515	28.664515	0.1378816	4.0300657	3.912	−55.734	63.621
(2, 11, 13)	−165.301620	29.396760	0.1425214	3.9009549	8.105	−51.497	67.848
(3, 10, 13)	−110.065450	29.803650	0.1466362	3.7933449	12.568	−46.999	72.372
(4, 9, 13)	−82.549293	29.802828	0.1500103	3.7095399	17.274	−42.267	77.171
(5, 8, 13)	−138.133930	29.330350	0.1524231	3.6518984	22.179	−37.346	82.199
(6, 7, 13)	−55.273449	28.359306	0.1536854	3.6224690	27.216	−32.302	87.382

this case the pattern is simple. Symmetrical patterns may also be constructed so that the points lie on two or more generative helices, in which case two or more points can be found on a circumference of the cylinder. Such patterns are said to have jugacy greater than 1 (*4*). Patterns with 2, 3, or *k* generative helices are bijugate, trijugate, or *k*-jugate. Unless otherwise stated, I will discuss only the simple, 1-jugate patterns.

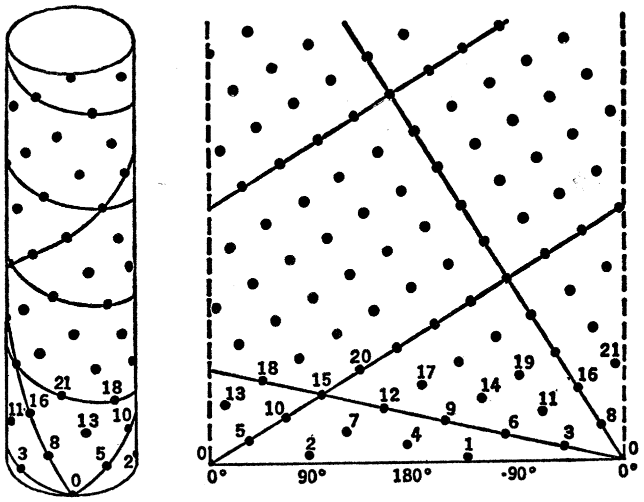

Fig. 1. A regular point set on a cylindrical surface, in perspective, and with the cylindrical surface unrolled into a plane. The generative helix is indicated by consecutive integers, 0, 1, 2 . . . , and 3-, 5-, and 8-parastichies, by solid lines.

When a pattern is specified by citing two sets of parastichies they will be referred to as the *m*- and *n*-parastichies, where *m* and *n* are integers. Referring to Fig. 1, one might take $m = 5$, $n = 8$, and note that one of the 5-parastichies connects points 0, 5, 10, 15 . . . , that is, that one of the *m*-parastichies connects points 0, *m*, 2*m*, 3*m* . . . . Another *m*-parastichy connects points 1, 6, 11, 16 . . . , or 1, $m + 1$, $2m + 1$, $3m + 1$ . . . , and so on, also for the set of *n*-parastichies, and other sets. It should be clear that there are *m m*-parastichies, and *n n*-parastichies.

In addition to *m* and *n*, which can be said to specify the symmetry properties of a pattern of points on a cylinder, other parameters are needed to specify its dimensions. One of these is the angle of rotation and another the length of the translation which constitute the screw displacement transforming point 0 to point 1. The first parameter is termed the angular divergence, and is designated α by Iterson (*2*). In this article α is given in degrees in Table 1 and the graphs, and in radians, ranging from $-\pi$ to π, in the equations. Values of the translational displacement, *h*, depend on the radius of the cylinder, *R*. Other parameters, such as the length of arc or chord between points, and the angle of inclination of a parastichy, can be derived from these.

Other derived parameters are concerned with screw displacements along *m*- and *n*-parastichies. (i) The vertical displacement, or translation, for the *m*-parastichies, from point 0 to *m*, from *m* to 2*m* . . . , is *mh*. Similarly, between successive points along *n*-parastichies, it is *nh*. (ii) The secondary divergence for the *m*-parastichies is the angular divergence from 0 to *m* . . . , and for the *n*-parastichies, from 0 to n . . . . If this is measured along the generative helix, it is $m\alpha$ for the *m*-parastichies, and $n\alpha$ for the *n*-parastichies. This may be a large angle, involving one or more circuits around the cylinder, and it will be convenient for some equations to subtract an integer multiple of 2π, the integer chosen to give the secondary divergence as the smallest angle, positive or negative, from point 0 to *m*, or from 0 to *n*. This smallest value of the secondary divergence will be symbolized δ_m, or δ_n, and formulated

$$\delta_m = m\alpha - 2t\pi$$
$$\delta_n = n\alpha - 2t\pi \qquad (1)$$

where the integer *t* in each case is so chosen that $-\pi < \delta_m \leqslant \pi$, for example. These equations are a statement of the familiar rules of trigonometry which are used in evaluating functions of large angles.

In general, it is not possible to draw spheres centered on the points of a cylindrical point set, so that they will pack uniformly. This is possible only with certain restrictions. From a consideration of packing of uniform spheres into a flat box, one restriction is clear, namely, that the points must be equidistant along two parastichies for rhombic packing, and along three for hexagonal packing (*5*).

Consider the arrangement of spheres which are in contact with each other, first along a single parastichy of a cylinder, then along two sets of parastichies (rhombic packing), then along three (hexagonal packing, or triple-contact arrangements). These are the subjectively evident parastichies, and the criterion for their selection is that the spheres which are centered on their points are tangent. They are contact parastichies, designated *m*, *n*, and $m + n$. In this case, *m* and *n* have no common divisor, and we choose $n > m$, except when $m = n = 1$.

In Fig. 2, the generative helix connecting point 0 and point 1 is shown, and two spheres, of radius, *r*, centered at the points 0 and *m*. The inclination of the generative helix to the circumference is β, and the vertical distance from point 0 to 1 is

$$h = R\alpha \tan \beta \qquad (2)$$

where *R* is the radius of the cylinder. The vertical distance to point *m* is $mh = mR\alpha \tan \beta$. This is the altitude of the right triangle (Fig. 2), whose hypotenuse is 2*r*, the distance between centers of two tangent spheres, and whose third side is also the base of the isosceles triangle, whose vertex is on the central axis of the cylinder and whose sides are radii of the cylinder.

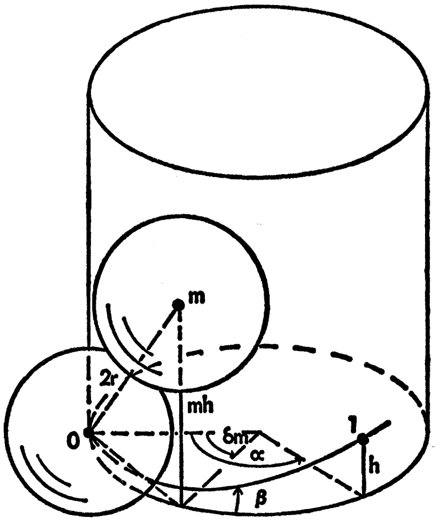

Fig. 2. Diagram of two tangent spheres, whose centers, 0 and *m*, are on the surface of a cylinder. The center of sphere 1 is also indicated. Symbols: α, angular divergence; *h*, translational displacement; δm, secondary divergence; 2*r*, distance between centers of two tangent spheres; β, inclination of generative helix to the circumference of the cylinder.

This third side is therefore $2R \sin \frac{1}{2} m\alpha$ or alternatively, $2R \sin \frac{1}{2} \delta_m$. The right triangle can then be solved to give

$$(r/R)^2 = \tfrac{1}{4}(m\alpha \tan \beta)^2 + \sin^2 \tfrac{1}{2} m\alpha \quad (3)$$

From similar consideration of spheres in contact along the n-parastichies

$$(r/R)^2 = \tfrac{1}{4}(n\alpha \tan \beta)^2 + \sin^2 \tfrac{1}{2} n\alpha \quad (4)$$

Solving these two equations simultaneously, one has

$$(m+n)(n-m)(\alpha \tan \beta)^2 = -4 \sin \tfrac{1}{2}(m+n)\alpha \sin \tfrac{1}{2}(n-m)\alpha \quad (5)$$

Equation 5 may be solved for values of α and $\alpha \tan \beta$, which will permit rhombic packing of uniform spheres, with contacts along the m- and n-parastichies. The ratio r/R can then be found from Eqs. 3 or 4.

However, Eq. 5 is not a sufficient condition for the construction of an arrangement of packed spheres, since it includes cases where the spheres intersect. The situation here may be understood by visualizing the rhombus (*5*) defined by the centers of spheres 0, m, n, and $m+n$, and that defined by 0, $n-m$, m, and n. The distances from 0 to $m+n$, and from 0 to $n-m$, must each be equal to or greater than the diameter of the spheres, $2r$, to assure that the spheres arranged along the parastichies $m+n$, or $n-m$, will not intersect. It may be helpful to consult Fig. 3, pattern (3, 5), where $m = 3$, $n = 5$, $n - m = 2$, $m + n = 8$. The distances from the centers of spheres 0 to 2, and from 0 to 8, are each greater than from 0 to 3, and from 0 to 5.

When the distance from 0 to $m+n$ equals $2r$, the spheres are in contact along the m-, n-, and $(m+n)$-parastichies, the pattern is a triple-contact, or hexagonal packing pattern, and it may be designated $(m, n, m+n)$. An example of this, with packing symmetry (3, 5, 8), is shown in Fig. 3, top right. To find values of α and $\alpha \tan \beta$ which apply to such a pattern, one first finds an equation similar to Eq. 5, for contacts along n- and $(m+n)$-parastichies

$$m(m+2n)(\alpha \tan \beta)^2 = -4 \sin \tfrac{1}{2}(m+2n)\alpha \sin \tfrac{1}{2} m\alpha \quad (6)$$

When Eq. 5 is divided by Eq. 6, $\alpha \tan \beta$ is eliminated

$$\frac{(m+n)(n-m)}{m(m+2n)} = \frac{\sin \frac{1}{2}(m+n)\alpha \sin \frac{1}{2}(n-m)\alpha}{\sin \frac{1}{2}(m+2n)\alpha \sin \frac{1}{2} m\alpha} \quad (7)$$

Similarly, when the distance from 0 to $(n-m)$ equals $2r$, one has the triple-contact pattern, $(n-m, m, n)$, with α defined by

$$\frac{n(2m-n)}{m(m+n)} = \frac{\sin \frac{1}{2}(2m-n)\alpha \sin \frac{1}{2} n\alpha}{\sin \frac{1}{2} m\alpha \sin \frac{1}{2}(m+n)\alpha} \quad (8)$$

These triple-contact patterns, $(n-m, m, n)$ and $(m, n, m+n)$, are limiting ones between which the double-contact pattern (m, n) exists. It is then of interest to solve these equations for values of α which characterize illustrative patterns. In practice, values of m and n are chosen in some systematic way, and values of α are obtained by solving Eq. 7. Then Eq. 5 is used to evaluate $\alpha \tan \beta$. The radius of the spheres, r, is taken as equal to 1. With this convention, R, the radius of the cylinder, can be found by substituting $\alpha \tan \beta$ into Eq. 3, and h, the translational displacement of spheres along the generative helix, can be found from Eq. 2.

The preceding paragraphs pertain to simple patterns, in which all of the spheres lie on a single generative helix. In multiple, or k-jugate patterns, upon which Iterson (*2*) did not elaborate, there are k generative helices, and the patterns have k-fold rotational symmetry, as well as screw symmetry, about the axis of the cylinder. The divergence along one of the generative helices will

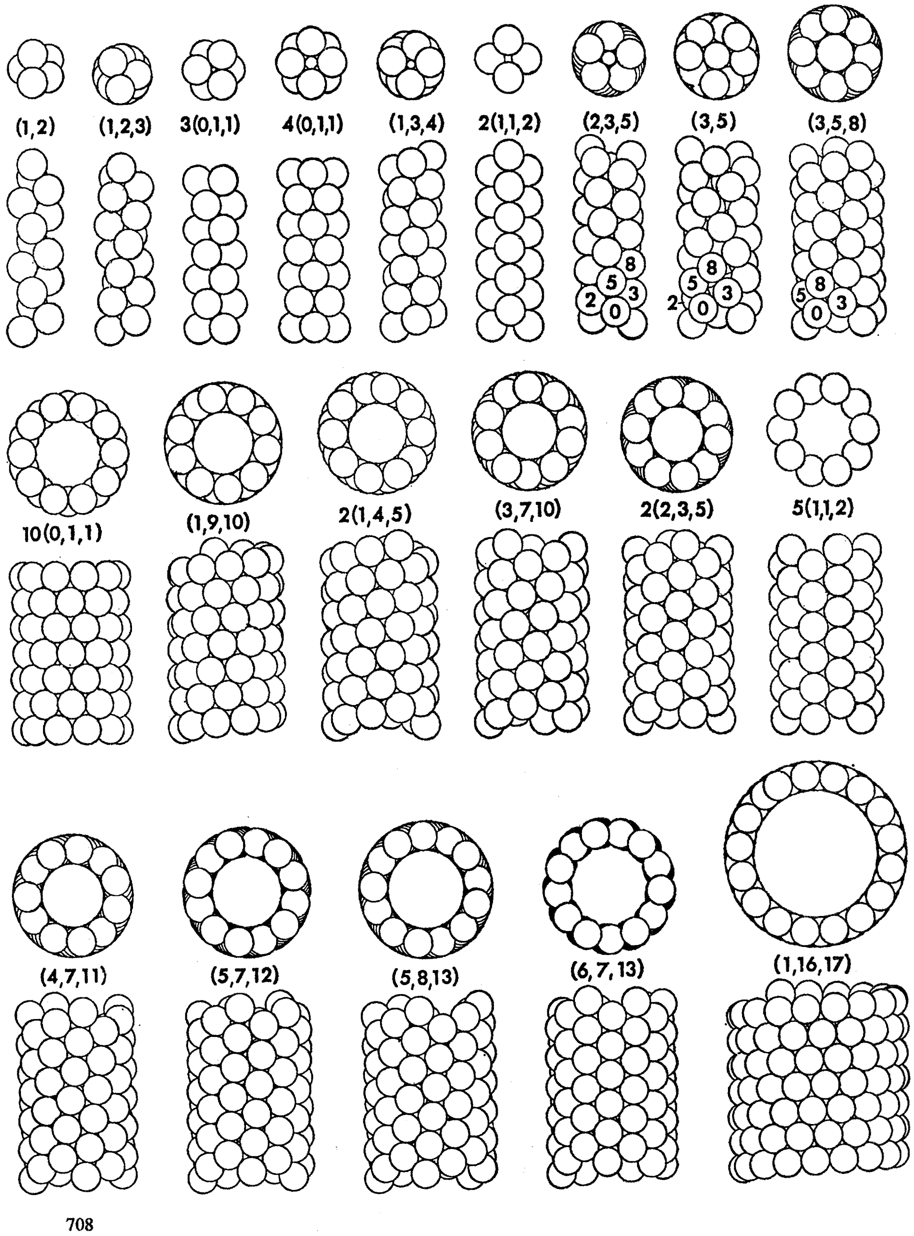

Fig. 3. Representative tubular arrangements of spheres, drawn in parallel projection onto the plane, in side view, and as viewed from above. All are triple-contact patterns, except (1, 2), with $\alpha = 144°$, $h = 0.8266$, and (3, 5), with $\alpha = 137.528°$, $h = 0.3358$. Parameters of other patterns are given in Table 1.

be referred to as α, and secondary divergences as $m\alpha$ or δ_m, and $n\alpha$ or δ_n. Since a k-jugate pattern is symmetrical on rotation through $2\pi/k$ radians, rather than 2π as in a simple pattern, the following counterparts of Eqs. 1 can be written

$$\begin{aligned}\delta_m &= m\alpha - 2t\pi/k \\ \delta_n &= n\alpha - 2t\pi/k \\ \delta_{m+n} &= (m+n)\alpha - 2t\pi/k \qquad (9)\end{aligned}$$

where the integer t, in each case, is chosen so that $-\pi/k < \delta_m \leqslant \pi/k$, for example. In the prior derivations, $2R \sin \frac{1}{2} m\alpha$, rather than $2R \sin \frac{1}{2} \delta_m$, was taken as the base of the isosceles triangle designated in Fig. 2. It is now more convenient to use δ_m, leaving this angle, δ_n and δ_{m+n} to be evaluated by Eqs. 9. With this modification, the same arguments, and the constructions of Fig. 2, apply to the k-jugate patterns, and the following equations for contacts along the m-, n- and $(m+n)$-parastichies are derived

$$\begin{aligned}(r/R)^2 &= \tfrac{1}{4}(m\alpha \tan\beta)^2 + \sin^2 \tfrac{1}{2}\delta_m \\ &= \tfrac{1}{4}(n\alpha \tan\beta)^2 + \sin^2 \tfrac{1}{2}\delta_n \\ &= \tfrac{1}{4}[(m+n)\alpha \tan\beta]^2 + \sin^2 \tfrac{1}{2}\delta_{m+n} \qquad (10)\end{aligned}$$

$$(m+n)(n-m)(\alpha \tan\beta)^2 = 4\sin^2 \tfrac{1}{2}\delta_n - 4\sin^2 \tfrac{1}{2}\delta_m \qquad (11)$$

$$\frac{(m+n)(n-m)}{m(m+2n)} = \frac{\sin^2 \frac{1}{2}\delta_m - \sin^2 \frac{1}{2}\delta_n}{\sin^2 \frac{1}{2}\delta_n - \sin^2 \frac{1}{2}\delta_{m+n}} \qquad (12)$$

On solving Eq. 12, one finds other parameters as outlined above for simple patterns.

Numerical Solutions of Equations

In general, Eqs. 7 and 12 cannot be solved directly, so that a numerical approximation method must be used. Some exceptional cases may be mentioned. In the (1, 2, 3) pattern, Eq. 7 can be simplified and solved directly to give $\alpha = 131.810°$. The pattern (1, 1, 2) is impossible, since it would require that sphere 0 be tangent to sphere 1 at two points. The triple contacts (0, 1, 1) and 2(0, 1, 1) are also impossible. The remaining whorled patterns, $k(0, 1, 1)$, $k \geqq 3$, exist, but for them Eq. 12 fails. In each whorl, the centers of the spheres define a regular plane polygon with k vertices, from which δ_0, and $\delta_1 = \alpha$, can be deduced. For $r = 1$, two special equations are derived by consideration of Fig. 2, $R = 1/\sin\alpha$, and $h^2 = 4(1 - \sin^2 \frac{1}{2}\alpha / \sin^2\alpha) = 4 - \sec^2 \frac{1}{2}\alpha$.

The interval-halving method of finding roots (*6*) was used for the remaining patterns, a routine based on Eqs. 9 being used to store values of α, δ_m, δ_n, and δ_{m+n} concurrently with each step of the iterative solution. Approximate starting values of α were obtained by a method which Iterson outlined (*7*). They might be found simply by trial.

The angle of inclination of the m-parastichies, μ, was found with the equation, $\mu = \tan^{-1}(mh/R\delta_m)$ (see Eq. 2), and similar equations were used for the inclinations of the n- and $(m+n)$-parastichies, ν and ϕ.

Table 1 lists the divergence angles, α, and several other parameters for a number of hexagonal patterns. They are arranged according to the number of longitudinal or near-longitudinal parastichies, or "strands," which they display. This number is the index $(m+n)$, or $k(m+n)$ in the designation of the pattern, and corresponds to the number of spheres which would appear in cross section. When the number of strands is prime, all of the patterns are simple, except the whorled patterns, $k(0, 1, 1)$, with k equal to the number of strands. When the number of strands is factorable, there are multijugate patterns corresponding to the factors (*8*, *9*). The list of patterns in Table 1 is complete to $k(m+n) = 13$, since it contains the possible combinations of km and kn (*10*).

In addition to the divergence, α, the secondary divergence, δ_m, is listed for each pattern. Each of the patterns, except $k(0, 1, 1)$ and $k(1, 1, 2)$, exists with right- and left-hand screw symmetry. The m-parastichies are arbitrarily considered to have right-screw symmetry, and δ_m is listed as a positive angle. In some patterns, the m-parastichies have the same handedness as the 1-parastichy and are said to be homodromous with it, and in others the m- and 1-parastichies are heterodromous. In the heterodromous cases, α is listed as a negative angle (*7*).

The fourth column in Table 1 lists h, the vertical spacing along the generative helix or helices, and the fifth lists R, the radius of the cylinder which is the locus of centers of the spheres, the radius of the spheres, r, being taken as unity. The outer diameter of the cylinder, that is, the outer envelope of the arrangement, is $2(R+1)$. The diameter of the cylindrical hole in the center of the figure, the inner envelope, is $2(R-1)$. If values of the radius other than unity are used, the listed values of h and R may be multiplied by this value to obtain actual dimensions of the model, corresponding to a real structure.

The last three columns of Table 1 give the angles of inclination to the circumference of the cylinder, μ, ν, and ϕ, of the m-, n- and $(m+n)$-parastichies. For each strand number, the whorled pattern, $k(0, 1, 1)$, has two sets of parastichies, n and $(m+n)$, running in opposite directions with inclinations approaching ± 60°. In the remaining patterns the strands become more nearly longitudinal as m becomes more nearly equal to n. In the pattern $k(1, 1, 2)$, the strand number, $k(m+n)$, is even and the strands are strictly longitudinal.

Some representative patterns in Fig. 3 illustrate these same relationships. Instructive models can be built of spherical beads, each with three holes spaced at 60° along the equator of the bead. They are strung with elastic cord, so that three cords (parastichies!) pass through each bead.

Rhombic or double-contact patterns, (m, n) or $k(m, n)$, can be solved by substituting appropriate divergence values into Eqs. 5 and 3, or Eqs. 11 and 10. These values of α, $\delta_m \ldots$, fall between those of the triple-contact patterns, $k(n-m, m, n)$ and $k(m, n, m+n)$, where $k \geqq 1$. It has not seemed worthwhile to tabulate values of α, h, and R for these double-contact patterns. Instead, R has been plotted against α in Fig. 4, for a number of patterns. This is related to graphs published by Iterson (*2*). In Fig. 4, it can be seen that an $(n-m, m, n)$ pattern can be transformed into an (m, n) pattern by decreasing h slightly, increasing R, and simultaneously either increasing or decreasing α. In the process, the contact between spheres 0 and $(n-m)$ is broken. By further decreasing h, increasing R, and coordinately changing α, a continuous transformation of (m, n) occurs, terminating in $(m, n, m+n)$. In general, a triple-contact pattern, $(m, n, m+n)$ can be transformed into any of the three double-contact patterns, (m, n), $(m, m+n)$, or $(n, m+n)$, by breaking the contacts, $m+n$, n, or m, respectively. This transformation is also illustrated in Fig. 3, upper right, where the (3, 5) pattern is seen as an intermediate in the transformation of the (2, 3, 5) pattern into the (3, 5, 8).

Higher order patterns that are not included in Table 1 can be approximated by a model of hexagonally packed circles on a cylindrical surface, if one equates the helical arc lengths between centers of circles, rather than the straight line distances between centers of spheres. A diagram of this model is shown in Fig. 5A, where a triangle is formed by the *m*- and *n*-parastichies intersecting at 120° at *mn*, and the circumference of the cylinder. The radius of the cylinder, *R*, can be found from the equation relating the sides of this triangle

$$2\pi R = 2rs$$

where r is the radius of the circles, and $s = \sqrt{m^2 + n^2 + mn}$. Equations for the parameters of this model are given without further derivation, in terms of the radical, s (*7, 11*)

$$\delta_m = (m + 2n)\pi/s^2,\ \delta_n = (2m + n)\pi/s^2$$

$$R = krs/\pi, \quad h = r\sqrt{3}/s$$

$$\mu = \cos^{-1}\left(\frac{m + 2n}{2s}\right),\ \nu = \cos^{-1}\left(\frac{2m + n}{2s}\right)$$

$$\phi = \mu + \pi/3 \tag{13}$$

The closeness of the approximation is indicated by the following values for the (5, 8, 13) pattern of circles of unit radius, which may be compared with the values for the (5, 8, 13) pattern of spheres in Table 1

$\delta_m = 29.302°$; $h = 0.15350$; $R = 3.61531$

$\mu = 22.411°$; $\nu = 37.589°$; $\phi = 82.411°$

Approximations can also be made graphically by drawing diagrams on isometric graph paper, and numbering the intersections of the coordinates which intersect at 60° with each other, as in Fig. 5A. Measurements made from the diagram, together with slide-rule calculations, may give satisfactory estimates of the parameters of the model of circles on a cylinder.

Application

If one considers the variety of patterns enumerated herein and the techniques available for investigating biological structures, it would seem that the most direct way to determine the packing symmetry of tubular structures would be to find (i) evidence that the packing is nearly hexagonal, (ii) the number of monomers which appear in a section perpendicular to the axis, and (iii) the angles of inclination of one or more sets of contact parastichies. Then by comparison with the spherical models (Table 1) it should be possible to make a choice. For instance, if it were found that a hexagonally packed structure were 13-stranded, one might choose the (4, 9, 13), (5, 8, 13), or (6, 7, 13) pattern depending on whether the inclination of the *m*-parastichies, μ, were closest to 17.3°, 22.2°, or 27.2°. The models are of spheres, and it is known that the monomers of many biological structures are markedly nonspherical. It is probably sufficient for applicability of this method that the monomers appear circular in a surface view of the tubule. Where the packing cannot be taken as hexagonal, as would be apparent in unequal spacing of the three sets of parastichies, the parameters of (m, n) or $k(m, n)$ patterns, as illustrated in Fig. 4, might be solved from Eqs. 5 or 11, for comparison with the data. However, simple geometric and numerical considerations should make it possible to decide the symmetry in nonhexagonal patterns, as described below.

Where the quality of the electron micrographs is not ideal, methods of enhancement of their rotational or translational periodicity are of value. Multiple photographic printing, with rotation or translation of the paper between exposures (*12*), has sometimes produced striking and convincing results. In other cases it has been equivocal. A stroboscopic method of enhancement of radial symmetry has also been described (*13*). To enhance the longitudinal periodicity it seems desirable to translate in the direction of the $(m + n)$-parastichies, rather than along the axis of the tubule.

Inoué has suggested that longitudinal views of these structures might be enhanced by viewing an electron micrograph through a Ronchi ruling placed in front of the eye (*14*). The Ronchi ruling can be turned to reinforce each set of contact parastichies in turn. The distance from the grating to the photograph should be adjusted so that the spacing produced by diffraction coincides with the spacing of the monomers. For nonhexagonal patterns the proper distance differs for the three sets of parastichies. At this distance, one can clearly distinguish reinforcements of the contact parastichies from reinforcements in other directions. A ruling with six or eight lines per millimeter (*15*) is suitable for viewing micrographs printed at magnifications of 1×10^5 to 3×10^5. It should be possible to take photographs through the ruling, and to make precise angular measurements of the reinforced photographs, but we have not explored this possibility.

A method of computer enhancement of rotationally symmetrical images has been described (*16*), in which the image is represented in computer storage as an array of optical density measurements from a film scanner. These are analyzed to provide a rotational power spectrum, that is, a plot of a radial power integral against rotational frequency. From this, it is possible for one to judge the frequency which best corresponds to the symmetry of the image, and to reconstruct the image in terms of the radial density distribution of an average sector, rejecting nonperiodic density variations which are presumably noise. This method has the advantage of providing an objective basis for deciding the number of monomers in the cross section—that is, the number of strands.

The optical diffraction method of analysis of tubules viewed perpendicular to the axis (*17, 18*) requires a consideration of the helical symmetry for its successful application, and should in theory provide one with a solution of the pattern. The original image can be reconstructed from the diffraction pattern (optical transform). Noise in the original image can be suppressed in the reconstruction, and, in particular, it is possible to obtain separate images of the two sides of a cylinder which are superimposed in the original. This is done by preparing masks which select spots corresponding to either the near or far side of the tubule.

The technical and analytical methods which are most appropriate to decide the pattern of arrangement of monomers in a particular cylindrical structure will differ from one case to another. To illustrate, I have analyzed published photographs and data on a number of tubular structures, referring to the models of spheres described herein. The analyses given below are intended only as suggestions of methods of analysis, and not as a comprehensive or critical review of this aspect of molecular morphology.

A bacteriophage tail. To illustrate the method of enhancement of electron micrographs by optical filtering, Klug and DeRosier (*17*) published a reconstructed image of the tail of an unidentified bacteriophage (their figure 5c). Two prominent intersecting sets of parastichies are visible, but the authors do not state how many there are. From the published illustration the inclinations of the parastichies were measured with an ordinary protractor. The m-parastichies, running to the left, gave a mean angle, $\mu = 27.37°$, with standard error, 0.33°, and the n-parastichies, running to the right, $\nu = 46.35° \pm 0.45°$. It was not possible to measure the $(m + n)$-parastichies with much confidence, but they appear to be at about 83°. Since $\mu + \nu = 73.72°$, rather than about 60°, the packing is not hexagonal, raising the question whether the m- and n-parastichies have the same spacing. Measurement gave a mean distance between units along the m-parastichies, $d_m = 1.177$ mm or 4.90 nm, and along the n-parastichies, $d_n = 1.167$ mm or 4.86 nm. The data of Table 1 and Fig. 4 are not applicable, but a graphical approximation to the pattern may be constructed by drawing a grid of parallel lines similar to those in Fig. 5A, with $\mu = 27.4°$, $\nu = 46.4°$, spaced in the ratio 1.177/1.167. With a little experimentation, the intersections were numbered with $m = 5$, $n = 8$, so that the line connecting the points marked 0, or other identical numbers, was very nearly horizontal, indicating that the pattern is (5, 8).

A more objective analysis can be devised by considering the triangle of Fig. 5A, two sides of which are the m- and n-parastichies which intersect at point 0 and again at point mn. Since there are n points along the m-parastichy, and m along the n-parastichy, the lengths of these sides, adjusted for the spacing of the parastichies, are in the ratio m/n. If one takes Q as an estimate of m/n

$$Q = (d_m \sin \mu)/(d_n \sin \nu) \qquad (14)$$

With the data given above, $Q = 0.641$, with 0.95 confidence limits, 0.625 and 0.657 (*19*). If one makes the liberal assumption that the number of strands, $(m + n)$, is between 9 and 17, one finds that the only pattern, whose ratio, m/n, lies within the confidence limits for Q, is (5, 8), and it seems certain that this illustration represents a (5, 8) rhombic pattern.

Turnip yellow mosaic virus. Hitchborn and Hills (*20*) described tubular structures which are formed in plants

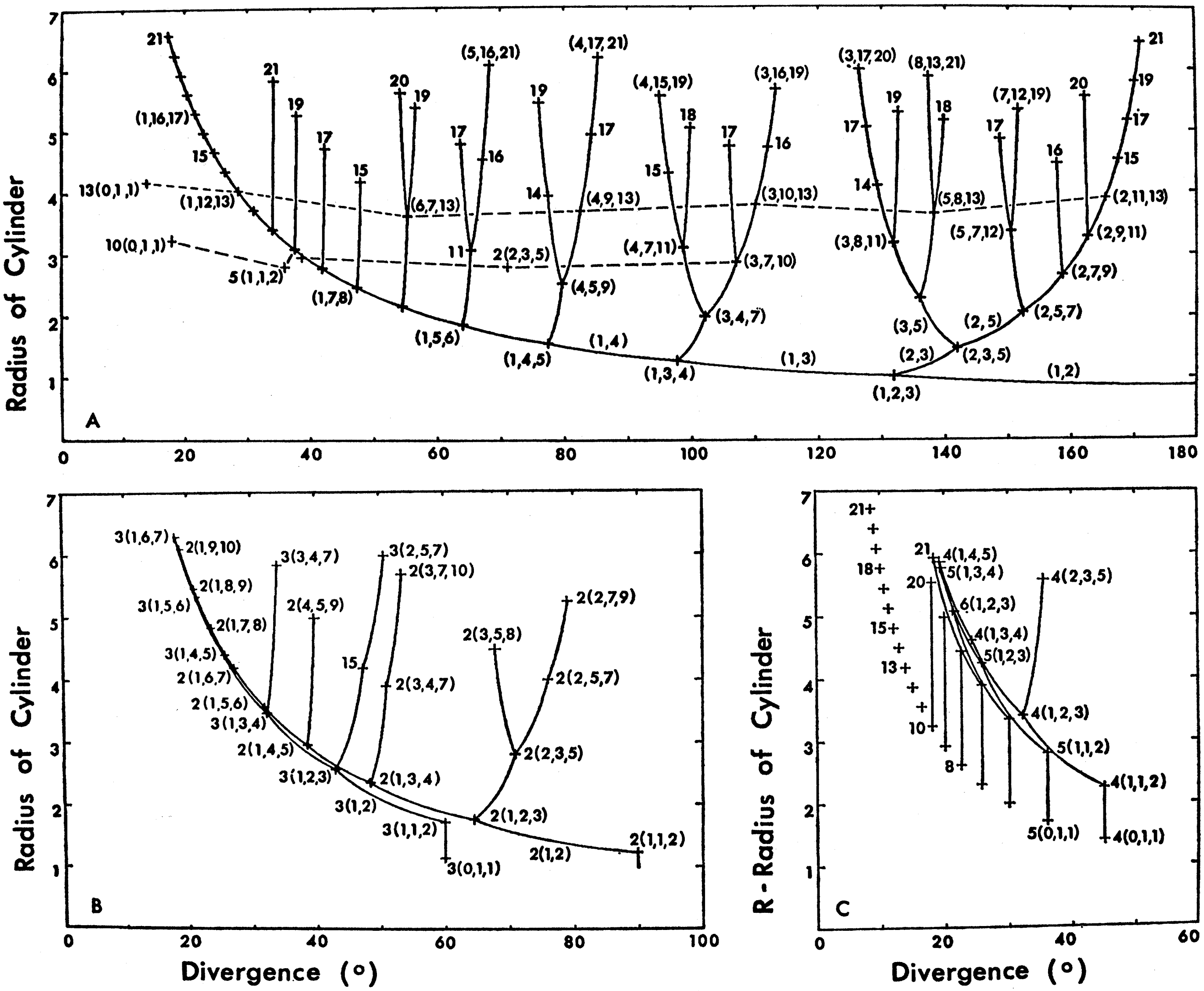

Fig. 4. Radius of cylinder R, plotted against divergence, α, for tubular arrangements of tangent spheres, with up to 21 strands. The spheres are of unit radius. The parameters of double-contact patterns are represented by arcs, labeled $k(m, n)$, and of triple-contact patterns, by pluses at the intersections of arcs, labeled $k(m, n, m + n)$. Some labels are omitted or abbreviated to strand number alone, $k(m + n)$. (A) Simple patterns, (B) bijugate and trijugate patterns, (C) k-jugate patterns with $k > 3$. In (A), the 10-strand and 13-strand triple-contact patterns are connected by dashed lines.

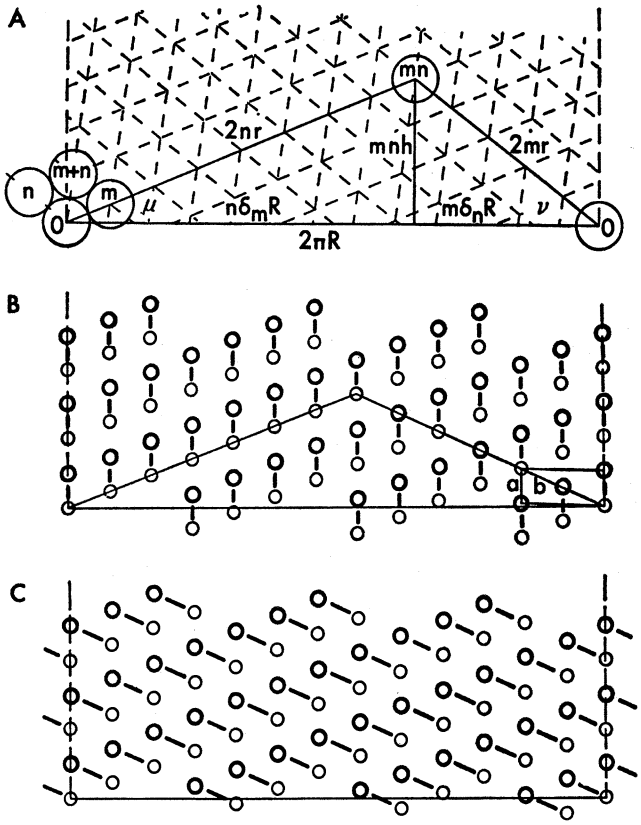

Fig. 5. (A) Diagram of circles hexagonally packed on the surface of a cylinder. Symbols: μ, angle of inclination of m-parastichies; ν, inclination of n-parastichies; other symbols defined in Fig. 2 and text. (B and C) Diagrams of the arrangement of monomers in a microtubule, based on chemical and x-ray diffraction data. Two classes of monomers, tubulins 1 and 2, shown as light and dark circles, are arranged along alternating 6-parastichies. The two possible arrangements of heterodimers are shown, with bonds along the 13-parastichies (B), and along the 7-parastichies (C). The rectangle in the lower right-hand corner of (B) represents the vertical and diagonal packing distances a and b, found by x-ray diffraction analysis (*39*).

infected with a necrotic strain of turnip yellow mosaic virus. Their electron micrograph, its optical transform, and a pattern obtained by rotating the micrograph through 60° in successive exposures, demonstrate an organization of the monomers into hexamers, which are themselves in a hexagonal configuration. The highest-order contact parastichies of these hexamers, $k(m+n)$, are inclined at 7° to the axis, implying the $\mu = 23°$, $\nu = 37°$. If one assumes that the structure was completely flattened on the grid, a comparison of the diameter of the tube with the 8.4-nm spacing of the hexamers gives an estimate of 42 strands. The parameters of 42-strand patterns are not listed in Table 1, but an estimate of m/n from Eq. 14, 0.649, suggests the pattern (17, 26, 43). Other patterns, such as 2(8, 13, 21) and 9(2, 3, 5) can be considered, but more precise measurements would be required for one to choose among them. The authors state that these tubules are not constant in diameter, and it is understandable that they may also vary in their contacts.

Polyheads of T4 bacteriophage. In their study of abnormal long tubular structures which are formed of head protein by a mutant of the bacteriophage T4D, DeRosier and Klug (*18*) presented electron micrographs and reconstructed images made from masked optical transforms of the micrographs. It appears that these tubules are formed within the bacterial cell as assemblages of concentric cylinders, which are separated during preparation for study. Therefore, tubules of several diameters are seen. The filtered images show a highly regular arrangement of hexamers, each consisting of six monomers at the vertices of a hexagon. I will discuss only the arrangement of the hexamers, although there are interesting questions of the more detailed structure. In an illustration of a tubule of about 80 nm diameter (*18*, plate II, lower right; my Fig. 6A) the mean inclinations of 10 m-, 10 n-, and 7 $(m+n)$-parastichies are $\mu = 22.88° \pm 0.09°$, $\nu = 36.06° \pm 0.17°$, $\phi = 82.36° \pm 0.06°$. Nine near-longitudinal parastichies appear in the illustration, so that one might assume that $k(m+n)$ is 20 or more. If one uses Eq. 14, Q is 0.6605 ± 0.0082. Of the patterns with $k(m+n)$ ranging from 18 to 28, only 4(2, 3, 5) and 5(2, 3, 5) have a ratio, $m/n = 0.6667$, which falls within the confidence limits for Q. The estimated angles, μ, ν, ϕ, also agree well with computed values for the 4(2, 3, 5) hexagonal pattern of spheres, 23.314°, 36.485°, and 83.335°. If it can be assumed that the tube was fully flattened, the pattern is 4(2, 3, 5). In another paper, these workers (*21*) show electron micrographs of several other polyheads. Analyzed in the same way, plates I and V of that paper are 2(3, 4, 7), plate III, top right, is either (6, 13, 19) or (7, 15, 22), and plate III, lower right, is 8(1, 2, 3). These images appear to be well worth further study.

Capsid of the bacteriophage ϕCbK. Leonard *et al.* (*22*) have analyzed the symmetry of the head or capsid of bacteriophage ϕCbK by optical diffraction of shadowed and negatively stained electron micrographs. The capsid consists of a tubule with a hexagonal packing pattern of units which appear from the chemical evidence to be made up of several proteins. It is capped at each end with an icosahedral dome. Measurements of the diameter of the tubule lead to an estimate of 15 near-longitudinal strands, and the authors present a model of sticks and plastic connectors, in which the tubule has the symmetry 5(1, 2, 3). (Their parameters, n, v, u, are identical with k, m, n, of this article.) In their model the cap conforms to the triangulation number, $T = 7$, which as noted (*11*) is identical with $s^2 = m^2 + n^2 + mn$, in Eq. 13 above.

In the micrographs and optical diffraction patterns of Leonard *et al.* (*22*, plate III), the inclination of the m-parastichies, μ, is about 11°, giving m/n about 0.25, and indicating that the pattern is 3(1, 4, 5), rather than 5(1, 2, 3) as they concluded. This tubule, which has threefold, rather than fivefold, rotational symmetry can also be capped by an icosahedral dome, with $s^2 = 7$, rotated so that a threefold vertex is at the pole, with the required six fivefold vertices symmetrically placed around it. In either model, the symmetry of the cap and of the cylindrical part of the capsid are closely related, and it would appear that a general study of the relationship of tubular and polyhedral packing patterns is in order.

Tobacco mosaic virus. The symmetry of arrangement of monomers in the protein coat of the tobacco mosaic virus appears to be well understood on the basis of x-ray diffraction analysis, biochemical studies, and the enhancement of electron micrographs by image rotation, optical diffraction and filtering, and computer analysis (*23*). It has the contact parastichies (1, 16, 17). In Klug and DeRosier's filtered image of one side of an electron micrograph (*17*, figure 4c), it is possible to compare the inclinations of the parastichies with the theoretical spherical model (Fig. 3). The 1-parastichy could not be measured confidently, but the other two angles are $\nu = 52.9° \pm 0.2°$, $\phi = 62.5° \pm 0.1°$, and can be compared with values computed for the model of spheres, $\mu = 2.98°$, $\nu = 56.82°$, $\phi = 62.81°$. The departure from regular hexagonal close packing is no doubt due to the well-documented nonspherical shape of the monomers.

Actin. Because of its importance as a constituent of muscle, actin has been studied extensively by a variety of techniques, of which the most pertinent to its ultrastructural symmetry are x-ray diffraction analysis and electron microscopy of purified preparations. Hanson and Lowy (*24*) present two models for F-actin, one based on their electron micrographs and the other on x-ray diffraction data of others. The models consist of two strands of monomers twisted 180° over a distance of 13 monomers in the electron micrographs, or 15 monomers in the x-ray preparations. In the terminology of this article, this is the double-contact pattern, (1, 2). This pattern (see Figs. 3 and 4) exists over a range of values of α, 131.8° to 180.0°, and of h, 0.632 to 1.00. Actin does not correspond to the fully extended (1, 2) pattern with $\alpha = 180.0°$, $h = 1.0$, nor is it likely that it can approach the limiting triple-contact configuration, (1, 2, 3) (Fig. 3). Whether the potential for extension and contraction, suggested by the geometric model, has any counterpart in the function of actin, is a matter on which I cannot comment.

Bacterial flagella. The flagella of *Salmonella* and several other genera of bacteria can be removed from the

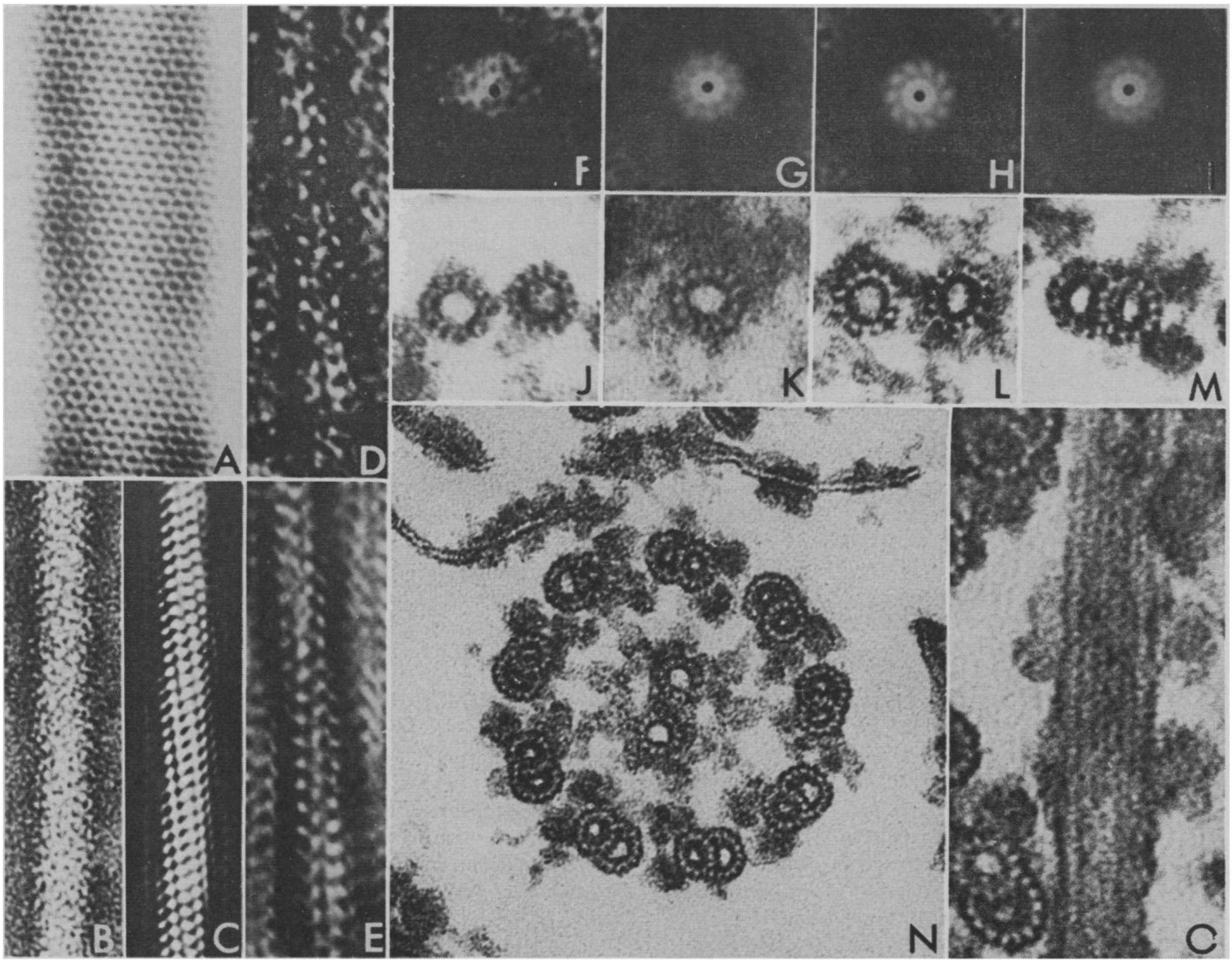

Fig. 6. (A) Optically filtered image of a polyhead of bacteriophage T4 (*18*), showing a 4(2, 3, 5) arrangement of hexamers, spaced about 10.0 nm along the parastichies. (B–I) Electron micrographs of straight flagella of *Salmonella*, showing a 2(2, 3, 5) arrangement of monomers; (B) negatively stained micrograph, (C) optically filtered image of (B), (D) negatively stained micrograph, and (E) the same micrograph enhanced by quadruple printing with translation by 5.2 nm parallel to an $(m + n)$-parastichy, between exposures. (F–I) Negatively stained transverse section of a flagellum (F), and the same micrograph multiply printed with rotation through 1/9 (F), 1/10 (G), and 1/11 (H) of 360° between exposures. Diameter = 17.5 nm. There are clearly ten strands. (J–O) Electron micrographs of microtubules, in which the arrangement of monomers is (6, 7, 13). (J) Transverse section of microtubules of the axoneme of *Echinosphaerium*. (K) Transverse section of a reconstituted microtubule of embryonic chick brain. (N) Transverse section of sperm tail of *Lytechinus pictus*, with membrane removed. (L–M) Details of central and outer fibers of (N). (O) Longitudinal section of an outer fiber of (N), in which reinforcement of the monomers can be seen with a Ronchi ruling. [(A) Reproduced from DeRosier and Klug (*18*) with permission of Academic Press; (B and C) from O'Brien and Bennett (*29*), with permission of Academic Press; (D–I) courtesy of Gerber and Routledge (*30*); (J–O) courtesy of Bryan and Tilney (*37*)]

cells and dissociated into monomers with a molecular weight of about 4×10^4. Studies of dielectric relaxation (*25*), low-angle x-ray scattering (*26*), and gel permeation chromatography (*27*) indicate that the molecules are elongate, having an axial ratio near 10. In negatively stained electron micrographs, the intact flagella present at least two well-marked patterns, referred to as the stranded and beaded appearances, in which the monomers appear to be organized either into longitudinal strands or into a helical configuration (*28*). Under suitable conditions, a solution of the monomers reaggregates to form filaments with apparently the same structure as the native flagella. In addition to the ultrastructural detail, the flagella usually have a long wavelength helical form, embracing several thousand monomers per gyre.

The *Salmonella* strain SJ814 is a mutant with straight flagella which appear to be particularly suitable for ultrastructural analysis. Using this mutant, O'Brien and Bennett (*29*) have made a study by optical diffraction of electron micrographs of negatively stained flagella, and published reconstructed images of the two sides of flagella. In their plate IIc (my Fig. 6C), a filtered image of one side of a flagellum, there is some lack of regularity, in that the angles μ and ν differ by 4° or 5° between the center of the figure and its top and bottom. Despite this, the 12 central m- and n-parastichies yield estimates, $\mu = 23.68° \pm 0.24°$, $\nu = 28.51° \pm 0.65°$, $d_m = 2.07$ mm, $d_n = 2.45$ mm. The sum, $\mu + \nu = 52.37° \pm 0.69°$, shows that the packing is not hexagonal. By using Eq. 14, $Q = 0.715$, with a 0.95 confidence interval, 0.679 to 0.751. The authors conclude (on inadequate evidence, I believe) that there are 11 strands. Of the patterns with 9 to 13 strands, only pattern (5, 7, 12), with $m/n = 0.714$, falls within the limits for Q. The pattern 2(2, 3, 5) should also be considered even though its ratio is less than 0.679, since the two 11-strand patterns (4, 7, 11) and (5, 6, 11), with ratios 0.571 and 0.833, respectively, are much further beyond the limits.

This *Salmonella* strain, SJ814, is under investigation by Gerber and Routledge (*30*). Figure 6F shows an example of a number of electron micrographs of sectioned flagella which have been enhanced by multiple printing with rotation through fractions of 360°, ranging from 1/4 to 1/14. In every case, rotation through 36°, 71°, or 72° gives the most satisfactory reinforcement, and gives evidence that there are ten strands (Fig. 6, G to I). Figure 6D is a side view of a negatively stained flagellum, and Fig. 6E is its enhanced image, made by quadruple printing with translation by 5.2 nm along an $(m+n)$-parastichy. Measurements of μ, ν, and the spacing in this enhanced photograph give 0.95 confidence limits for m/n, 0.592 to 0.694, which clearly indicate that the pattern is 2(2, 3, 5). Similar analysis of several other micrographs leads to the same conclusion.

Viewed through the Ronchi ruling, micrographs of these flagella show reinforcement of the 2- and 3-parastichies, both to the right and to the left at the predicted angles, 23° and 36°, as nearly as can be judged. It would require only a slight transformation of the 2(2, 3, 5) pattern to break the contacts along the 3-parastichies and tilt the 5-parastichies into a strictly longitudinal orientation, producing the stranded appearance. I have examined a considerable number of published and unpublished micrographs of *Salmonella* flagella and find the appearance of the parastichies consistent in all.

It is most interesting that Harris and Scriven (*31*) present a photograph of a 2(2, 3, 5) model made of rubber balls to illustrate their theory that dislocations may account for the long wavelength curvature of normal flagella of *Salmonella*.

There is undoubtedly a variety of patterns of flagellar organization among the bacteria, as Asakura (*32*) has indicated. In *Escherichia coli*, Grund (*33*) has provided illustrations of flagella prepared by freeze-etching and heavy metal shadowing. The parastichies in his micrographs are at about 60°, and appear therefore to be n and $(m+n)$, so that m has a low inclination. The number of strands is apparently not known, but one might hazard a guess that the pattern is (1, 8, 9), (1, 9, 10), or (1, 10, 11).

Microtubules. Microtubules have been described from the cells of a large number of eukaryotic organisms, and appear to play a variety of roles in cell architecture and function. Until quite recently there appears to have been little information on the packing symmetry of monomers in these structures. However, Ledbetter and Porter (*34*) and Porter (*35*) published unequivocal micrographs demonstrating 13 subunits in cross sections of microtubules in a conifer, *Juniperus chinensis*, and an angiosperm, *Euphorbia milii*, due apparently to a natural negative staining effect. The clarity of the images suggests that ϕ must be high, as in (5, 8, 13) or (6, 7, 13). Figure 6J shows a negatively stained section of two microtubules of the axoneme of *Echinosphaerium nucleofilum* (*36, 37*). Figure 6K is a section of a reconstituted microtubule from embryonic chick brain (*37*). Both of these micrographs show 13 subunits clearly.

The flagella and cilia of eukaryotes are complex structures consisting of nine outer fibers, which themselves are complex, and two inner fibers, with an outer membrane and other structures (*38*). The outer fibers consist of two connected tubules, the A subfibers which are cylindrical and the B subfibers which are incomplete cylinders attached laterally to the A subfibers. Figure 6N is an electron micrograph of a section of a sperm tail of the sea urchin *Lytechinus*, with the flagellar membrane removed (*37*). There are clearly 13 subunits in the circular sections of the A subfibers, 11 in the B subfibers (Fig. 6M), and 13 in the two central singlets (Fig. 6L).

Cohen *et al.* (*39*) have studied purified samples of the A tubule of outer fibers of sperm tails of the sea urchin *Strongylocentrotus* by x-ray diffraction and proposed either a 12- or 13-stranded structure, the adjacent strands alternately half-staggered. The packing distances which Cohen *et al.* propose, $a = 4.0$ nm for the vertical spacing, and $b = 5.3$ nm, the diagonal distance to the centered unit (Fig. 5B), imply that the pattern is either 6(1, 1, 2) or (6, 7, 13), as in their diagrams. It is not a regular hexagonal pattern, however, since that would require that $a = b$.

Side views of flagellar outer fibers, such as those of Grimstone and Klug (*40*) of the flagellate *Trichonympha*, and longitudinal sections such as in Fig. 6O indicate that the 13-parastichies are strictly longitudinal. With this fact and the dimensions provided by Cohen *et al.* (*39*), an approximate model of the microtubules can be constructed. Since $\delta_{13} = 0°$, $\alpha = 55.385°$ (Eq. 1). The subunits are most closely spaced, 4.0 nm, along the 13-parastichies, and next most closely along the 6-parastichies, as can be seen in the diagrams, Fig. 5, B and C. If one assumes that 5.3 nm is the average spacing along the 6- and 7-parastichies, the triangle of Fig. 5B can be solved to give $d_6 = 5.24$ nm, $d_7 = 5.36$ nm, and the radius, $R = 10.55$ nm, which agrees with the outer and inner radii, 11.6 and 8.5 nm, given by Cohen *et al.* (*39*). The inclinations of the 6- and 7-parastichies are nearly equal, $\mu = 20.6°$ and $\nu = 23.7°$. It is possible to see reinforcement of subunits along these parastichies with the Ronchi ruling in many micrographs of microtubules from various sources. However, the inclination of the superimposed 6- and 7-parastichies is usually about 19°, rather than about 22°, as predicted from the model. This agrees with Thomas's data (*41*), and suggests some distortion in the electron micrographs. This model does not take into account the indication of x-ray diffracting features at different radii, the detailed relationship of the A and B subfibers, and other complexities.

Chemical studies have shown that the protein of flagellar microtubules dissociates into dimers, which can be separated by gel electrophoresis into two components which differ somewhat in their amino acid composition and other properties (*42*). The two monomers apparently occur in equal amounts in both the A and B subfibers, and this has prompted some speculation about the disposition of the monomers, or dimers, in the tubules (*43*). If one assumes that the two monomers are symmetrically arranged, a consideration of the (6, 7, 13) pattern shows that the two types must alternate along the odd-numbered, 7- and 13-parastichies, and that monomers of one type must be arrayed along a given 6-parastichy, and of the other type along the adjacent 6-parastichy, as indicated by light and heavy circles in Fig. 5, B and C. This agrees with a diagram of Stephens (*44*). If one assumes that there is preferential heterodimer bonding in the assembled microtubule (*42*), there appear to be two possible symmetrical positions for the bonds. They may be longitudinal, lying along the 13-parastichies (Fig. 5B), or along the 7-parastichies, connecting monomers of the two types which belong to adjacent 6-parastichies (Fig. 5C) (*45*). I do not know of any evidence which would permit a choice between these two models. Both models have polarity, as shown in the diagrams by the fact that the heavy circle in each pair is consistently toward the top of the page. It is interesting to note that Subirana (*46*) has presented arguments that the microtubules of the mitotic spindle must have this property.

Summary

The symmetrical arrangements of monomers into such cylindrical structures as microfilaments of actin, flagella of bacteria, microtubules of many organisms, and the protein coats of viruses can be specified by citing the index numbers of two or three sets of contact parastichies, or helical ranks of monomers, as has been done in classical studies of phyllotaxis. This specification has the form $k(m, n)$ or $k(m, n, m+n)$, where m, n, and $(m+n)$ are parastichy numbers specifying screw displacements, and k is the jugacy, or frequency of rotational symmetry. For simple structures, $k = 1$. This notation has the advantage of terseness and of indicating the basic isometries of these helically symmetrical structures.

Theoretical models of the packing of spheres whose centers lie on the surface of a cylinder have been investigated geometrically. Their symmetry properties are discussed. Parameters of these models, such as the angular divergence, α, the longitudinal displacement between successive spheres, h, the radius of the cylinder, and the angles of inclination of the parastichies, have been computed for representative patterns.

The ultrastructural symmetry of several biological structures of this sort has been inferred by comparison with these models. Actin, for example, has the symmetry (1, 2), *Salmonella* flagella, 2(2, 3, 5), the tobacco mosaic virus, (1, 16, 17) and the microtubules of many higher organisms, (6, 7, 13).

References and Notes

1. H. S. M. Coxeter, *Introduction to Geometry* (Wiley, New York, 1961).
2. G. van Iterson, *Mathematische und Mikroskopisch-Anatomische Studien über Blattstellungen* (Fischer, Jena, 1970). Iterson cites earlier work by Airy, Delpino, and Schwendener on cylindrical packing of spheres, but I am not aware of more recent references. It is appropriate that I mention Prof. van Iterson's death 4 January 1972, at age 94.
3. H. Weyl, *Symmetry* (Princeton Univ. Press, Princeton, N.J., 1952).
4. Note by A. M. Turing, published posthumously in S. Turing, *Alan M. Turing* (Heffer, Cambridge, England, 1959), p. 141.
5. In describing patterns of points on a cylindrical surface, the parastichies were considered as cylindrical helices. In the arrangements of spheres, the points of contact are not on such helices, but on straight line segments between their centers. It is therefore not strictly correct to speak of spheres which are "in contact along a single parastichy," for example, but this loose terminology will be used for brevity. Alternatively, a parastichy might be defined as the polygonal sequence of straight line segments connecting the centers of a rank of spheres. The use of the terms rhombic and hexagonal packing is similarly loose, since the rhombus and hexagon are ordinarily understood to be figures in a plane.
6. D. D. McCracken and W. S. Dorn, *Numerical Methods and Fortran Programming* (Wiley, New York, 1964).
7. Equations 1 and 9 can be put more explicitly in the form, $\delta_m = m\alpha - \Delta m(2\pi/k)$, where Δm is an encyclic number, the number of circuits of the cylinder divided by k, from point 0 to point m, along the 1-parastichy, rounded to the nearest integer. Likewise, $\delta_n = n\alpha - \Delta n(2\pi/k)$. For given m and n, Δm and Δn are the smallest integer solutions, ≥ 0, of the diophantine equation, $m\Delta n - n\Delta m = \pm 1$. Crude approximations of α, in triple-contact patterns, are given by $(\Delta m/m)(2\pi/k)$ and $(\Delta n/n)(2\pi/k)$. To find the values of α for the model of hexagonally packed circles on a cylinder, two cases must be considered. If $m\Delta n - n\Delta m = 1$, the m-parastichy has the same chirality as the 1-parastichy, and
$$\alpha = \left(\frac{\Delta m}{m} + \frac{m+2n}{2ms^2}\right)\frac{2\pi}{k}$$
If $m\Delta n - n\Delta m = -1$, the m-parastichy is heterodromous with the 1-parastichy, and
$$\alpha = \left(\frac{\Delta n}{n} + \frac{2m+n}{2ms^2}\right)\frac{2\pi}{k}$$
In solving the equations for the model of spheres packed on the surface of a cylinder, these values of α, incremented and decremented by arbitrary small amounts, serve as initial values in the interval-halving routine. Iterson (*2*) gives a full exposition of these relationships.
8. M. F. J. Moody, *J. Mol. Biol.* **12**, 342 (1967). Moody alludes to this relationship by stating a theorem, which he attributes to D. W. Thompson (*9*).
9. D. W. Thompson, *On Growth and Form* (Cambridge Univ. Press, London, 1952).
10. The classical discussions of phyllotaxis are closely tied up with the Fibonacci sequence, 0, 1, 1, 2, 3, 5, 8 . . . , and other additive sequences, such as, 1, 3, 4, 7 . . . , in which each term is the sum of the preceding two. The indices, m and n, are typically considered as two successive terms of such a sequence. If quotients are formed of successive pairs of Fibonacci numbers, an alternating sequence is formed, 1/1, 1/2, 2/3 . . . , which converges to the golden mean. This is the positive root of the equation $\chi^2 + \chi - 1 = 0$, and has the value 0.6180340. It has frequently been asserted that the leaves of higher plants are initiated with an angular divergence equal to the Fibonacci angle, which is $(1 - \chi)$ 360°, or 137.508°. It is not at all clear to me whether this numerology has any pertinence to the assembly or function of submicroscopic structures [H. S. M. Coxeter, *J. Algebra* **20**, 167 (1972), and the references which he cites].
11. The integers $P = m^2 + n^2 + mn$ appear in the discussion of triangle-faced polyhedra as models of the symmetry of polyhedral viruses. "Triangulation numbers," $T = Pf^2$, where f is an integer, are recommended to specify particular patterns. It should be preferable to cite m and n, since there are distinct patterns which have the same value of s^2, for example, (1, 9, 10) and (5, 6, 11), both with $s^2 = 91$. [D. L. D. Caspar and A. Klug, *Cold Spring Harbor Symp. Quant. Biol.* **27**, 1 (1962); H. S. M. Coxeter, in *A Spectrum of Mathematics*, J. C. Butcher, Ed. (Auckland Univ. Press, Auckland, New Zealand, and Oxford Univ. Press, London, 1971)].
12. R. Markham, J. H. Hitchborn, G. J. Hills, S. Frey, *Virology* **22**, 342 (1964).
13. R. Markham, *Collect. Pap. Annu. Symp. Fundam. Cancer Res.* **17**, 180 (1963).
14. S. Inoué, personal communication.
15. Edmund Scientific Co., Barrington, N.J. 08007.
16. R. A. Crowther and L. A. Amos, *J. Mol. Biol.* **60**, 123 (1971).
17. A. Klug and D. J. DeRosier, *Nature* **212**, 29 (1966).
18. D. J. DeRosier and A. Klug, *J. Mol. Biol.* **65**, 469 (1972).
19. The standard error of Q was estimated from those of μ and ν, in radians, by a propagation of error formula
$$s_Q{}^2 = \left(\frac{\partial Q}{\partial \mu}\right)^2 s_\mu{}^2 + \left(\frac{\partial Q}{\partial \nu}\right)^2 s_\nu{}^2$$

[see H. D. Young, *Statistical Analysis of Experimental Data* (McGraw-Hill, New York, 1962)].
20. J. H. Hitchborn and G. J. Hills, *Science* **157**, 705 (1967).
21. M. Yanagida, D. J. DeRosier, A. Klug, *J. Mol. Biol.* **65**, 489 (1972).
22. K. R. Leonard, A. K. Kleinschmidt, N. A. Keshishian, L. Shapiro, J. V. Maizel, *ibid.* **71**, 201 (1972).
23. A. Klug, *Fed. Proc.* **31**, 30 (1972).
24. J. Hanson and J. Lowy, *J. Mol. Biol.* **6**, 46 (1963).
25. B. R. Gerber, L. M. Routledge, S. Takashima, *ibid.* **71**, 317 (1972).
26. W. Bode, J. Engle, D. Winklmair, *Eur. J. Biochem.* **26**, 313 (1972).
27. B. R. Gerber and H. M. Robbins, *Biophys. Soc. Annu. Meet. Abstr.* **11**, 102a (1971).
28. J. Lowy and J. Hanson, *J. Mol. Biol.* **11**, 293 (1965).
29. E. J. O'Brien and P. M. Bennett, *ibid.* **70**, 133 (1972).
30. B. R. Gerber and L. M. Routledge, unpublished data.
31. W. F. Harris and L. E. Scriven, *J. Mechanochem. Cell Motility* **1**, 33 (1971). I found this and other basically important articles by Harris on "cylindrical crystals" only after completion of this article.
32. S. Asakura, *Advan. Biophys.* **1**, 99 (1970).
33. S. Grund, *Zentralbl. Veterinaermed. Reihe B* **18**, 133 (1971).
34. M. C. Ledbetter and K. R. Porter, *Science* **144**, 872 (1964).
35. K. R. Porter, in *Principles of Biomolecular Organization*, G. E. W. Wolstenholme and M. O'Connor, Eds. (Churchill, London, 1966), p. 308.
36. L. G. Tilney, *J. Cell Biol.* **51**, 837 (1971).
37. ——— and J. Bryan, unpublished data.
38. I. R. Gibbons and A. V. Grimstone, *J. Biophys. Biochem. Cytol.* **7**, 697 (1960).
39. C. Cohen, S. C. Harrison, R. E. Stephens, *J. Mol. Biol.* **59**, 375 (1971).
40. A. V. Grimstone and A. Klug, *J. Cell Sci.* **1**, 351 (1966).
41. M. B. Thomas, *Biol. Bull. Woods Hole* **138**, 219 (1970).
42. J. Bryan and L. Wilson, *Proc. Nat. Acad. Sci. U.S.A.* **68**, 1762 (197 → I. Meza, B. Huang, J. Bryan, *Exp. Cell Res.* **74**, 535 (1972); J. Bryan, *J. Mol. Biol.* **66**, 157 (1972).
43. G. B. Witman, K. Carlson, J. L. Rosenbaum, *J. Cell Biol.* **54**, 540 (1972).
44. R. E. Stephens, in *Cilia and Flagella*, M. A. Sleigh, Ed. (Academic Press, London, in press).
45. This conclusion is tentative. If the dimers, rather than the monomers, are numbered consecutively along a 1-parastichy, it turns out that the arrangement is (3, 10, 13). It would be interesting to explore the symmetrical tubular arrangements of two or more classes of objects.
46. J. A. Subirana, *J. Theoret. Biol.* **20**, 117 (1968).
47. I am grateful to my colleagues, Bernard R. Gerber, Lewis M. Routledge, Lewis G. Tilney, Joseph Bryan, and Shinya Inoué for prodding me to consider this problem, and for providing references, data, and critical discussion. Arthur Veen has offered mathematical criticism and has carried out most of the computer solutions of equations and computer plotting of figures. This work has had the support of grant GB-23028 from the National Science Foundation.

The Dynamics of a Heroin Addiction Epidemic

Heroin abuse has declined in Washington, D.C.

Robert L. DuPont and Mark H. Greene

In the mid-1960's a wave of heroin addiction enveloped Washington, D.C., and directly affected the lives of an estimated 18,000 residents of that city. Almost every other major metropolitan area in the United States witnessed a similar phenomenon, with associated criminal activity and social disruption. In response to the obvious need to bring the heroin addiction problem under control, a variety of treatments and intervention strategies were developed throughout the country. The debate regarding the effectiveness of addiction treatment, the role of law enforcement, the value of methadone, and the motives of treatment planners has been characterized by more heat than light and continues unabated and unresolved.

The District of Columbia made a major manpower and monetary commitment in an attempt to solve its heroin addiction problem. There were two components to its intervention strategy. The first was a comprehensive, multimodal treatment program for addicts, which began in the fall of 1969 and relied substantially, but not exclusively, on methadone (*1*). The second was a major law enforcement commitment to reduce the supply of heroin in the city, which also began in 1969 (*2*). Observations made during the 3 years since the implementation of these programs form the basis for this article.

In early 1973, the heroin epidemic appeared to be waning in the District of Columbia. In this article we document the decline of heroin addiction in the nation's capital, using measures of the incidence and prevalence of heroin addiction, as well as measures of the availability, cost, and quality of heroin in the streets. It is our intention to describe what has happened in Washington, D.C., during a time in which intensive efforts have been directed at solving the problem of heroin addiction.

Methods

Few data on heroin use were gathered in the District of Columbia before 1969. Since then, data have been systematically collected and analyzed from a number of sources. Some data have been available since 1969. Other data only became available as our understanding of the addiction problem developed. The following sources were used during this analysis.

Patients in treatment. Starting in July 1970, information on the year and age of first heroin use has been tabulated for all patients entering the Narcotics Treatment Administration (NTA), the city's comprehensive addiction treatment program. Monthly totals of the number of patients entering treatment have been available since October 1971. This information is subdivided according to type of patient referral (voluntary or criminal justice) and to whether the patient is new to NTA or is being readmitted to treatment. Periodic surveys have been made to elicit information regarding the street availability and quality of heroin as judged by addicts entering treatment. Questionnaire information obtained from addicts has been shown to be remarkably reliable (*3*).

Urine drug testing. Urine testing for heroin has been carried out at three locations. Heroin use is indicated by the presence of morphine or quinine or both in the urine. Arrestees held in the

---

Dr. DuPont is director of the Special Action Program Office for Drug Abuse Prevention, Washington, D.C. 20500. Dr. Greene is the epidemic intelligence service officer at the Center for Disease Control, Atlanta, Georgia 30333.